Light Metals 2015
Edited by: Margaret Hyland
TMS (The Minerals, Metals & Materials Society), 2015

INFLUENCE OF PARTIAL SUBSTITUTION OF Cu BY VARIOUS ELEMENTS IN Cu-Ni-Fe ALLOYS ON THEIR HIGH-TEMPERATURE OXIDATION BEHAVIOR

E. Gavrilova[1], G. Goupil[1], B. Davis[2], D. Guay[1] and L. Roué[1]

[1] INRS-Énergie, Matériaux et Télécommunication, 1650 Blvd Lionel-Boulet, Varennes (QC) J3X 1S2 Canada
[2] Kingston Process Metallurgy Inc.; 759 Progress Avenue, Kingston, Ontario, K7M 6N6, Canada

Keywords: Al electrolysis, inert anode, Cu-Ni-Fe based alloys, mechanical alloying, high-temperature oxidation

Abstract

The effect on the high temperature oxidation behavior of partially substituting Cu by M, with M = Sn, Ag, V, Nb, Ir, Ru, Ta, in mechanically alloyed Cu-Ni-Fe anode was investigated. Characterization of the as-milled and consolidated powders was achieved through a combination of XRD, SEM and EDX mapping. On the basis of TGA experiments performed at 700°C under oxygen and subsequent SEM-EDX analyses, substitution of Cu by Nb, Ru, Ir, Sn and Ag leads to the formation of thinner Cu oxide layers at the surface of the electrode. However, except for M = Nb, chemical segregation was observed in the bulk alloy.

Introduction

Among the various metallic materials that have been explored as inert anodes for Al electrolysis, Cu-Ni-Fe based alloys appear as the most promising [1-5]. This is mainly due to their ability to form a protective surface layer of $NiFe_2O_4$ during Al electrolysis, which is recognized for its low solubility in cryolite media [6]. For instance, O-doped $Cu_{65}Ni_{20}Fe_{15}$ alloy produced by mechanical alloying has good corrosion resistance in low temperature (700°C) KF-AlF_3-based electrolyte with a wear rate estimated at 0.8 cm $year^{-1}$ leading to the production of Al with a purity of 99.8 % [5].

We have shown that Cu in mechanically alloyed Cu-Ni-Fe anodes plays a key role in the formation of a protective $NiFe_2O_4$–rich layer [5]. As a result, Cu-Ni-Fe anodes with a Cu content lower than 50-60 wt% are unstable for Al electrolysis. A possible explanation is that the CuO_x rich-layer formed at the surface of the anode during the first stage of the Al electrolysis acts as a "sacrificial layer" which may give time for the inner formation of a coherent $NiFe_2O_4$ scale. The fact that the diffusion coefficients of Ni and Fe in Cu-Ni-Fe alloys increase with their Cu content [7] may also favor the formation of $NiFe_2O_4$. However, Cu leaching from the Cu-Ni-Fe anodes into the cryolite bath has a negative impact on the purity of the produced Al in the short term in addition to creating pathways for deleterious electrolyte penetration into the anode surface scale in the longer term [8].

To overcome this issue, partial substitution (5 wt%) of Cu in $Cu_{65}Ni_{20}Fe_{15}$ alloy by various elements (Sn, Ag, V, Nb, Ir, Ru, Ta) selected on the basis of their low solubility in cryolite media is performed in the present work. As a first step toward their evaluation, the high temperature oxidation behavior of these quaternary alloys is investigated and compared to that of ternary Cu-Ni-Fe alloy.

Experimental

$Cu_{60}M_5Ni_{20}Fe_{15}$ (in wt%) alloys with M = Sn, Ag, V, Nb, Ir, Ru, Ta were prepared by ball milling using a vibratory-type miller (Spex). 11.5 g of elemental Cu, Ni, Fe and M powders (purity ≥ 99.9%, -325 mesh) in appropriate proportion were introduced in a stainless steel vial (capacity of 55 ml) containing two 14 mm diam. and one 11 mm diam. stainless steel balls, corresponding to a ball-to-powder mass ratio (BPR) of 2:1. 0.5 wt.% of stearic acid was added to the initial mixture as process control agent to prevent excessive cold-welding on the milling tools. The milling was performed for 10 h under Ar atmosphere. The composition of the as-milled powders determined by energy dispersive X-ray (EDX) analysis was in accordance (within 1.5 wt%) with their nominal composition.

Powder consolidation was carried out to obtain dense disc samples for the oxidation tests. The as-milled powder was firstly sieved to select only the powder fraction with a particle size of 20 to 75 µm. This sieved powder was placed in a quartz cylinder preform and heated from room temperature to 1000°C under Ar atmosphere (softening treatment). The resulting sample was cold pressed at 18 tons cm^{-2} for 10 min and then sintered at 1000°C under Ar atmosphere for one hour. The final pellet had a diameter of 11.5 mm and a thickness of ~1.5 mm with a weight of ~1 g.

The crystalline structure of the as-milled and consolidated powders was determined by X-ray diffraction (XRD) using a Bruker D8 diffractometer with Cu K_α radiation. Their morphology was characterized using a JEOL JSM-6300F scanning electron microscope (SEM) in backscattered electron (BSE) mode.

The high temperature oxidation tests were carried out using a thermogravimetric analyser (TGA) (Thermax 500) at 700°C under Ar-20%O_2 for 20 h. After oxidation, the samples were analyzed by XRD and SEM-EDX mapping.

Results and discussion

Figures 1A and 1B show the XRD patterns of the as-milled and consolidated Cu-Ni-Fe-M materials, respectively. As shown in Figure 1A, in all cases, the XRD pattern is mainly constituted of a series of peaks, which corresponds to a face-centered-cubic (fcc) phase attributed to a solid solution of Cu(Ni,Fe,M) named γ-phase. However, for M = Ir, Ru and Ta, small additional peaks are discernible, which can be attributed to the presence of unalloyed M. The fact that no peak associated with pure M elements is discernable for M = Sn, Ag, V and Nb suggests that the alloying process is completed with these elements but it may also be due to the small size of the M crystals dispersed in the Cu(Ni,Fe) matrix.

However, in all cases, a small shift towards the lower 2θ angles of the diffraction peaks of the γ phase compared to those of the ternary Cu-Ni-Fe alloy is observed, suggesting that the alloying process with all M elements is at least initiated after 10 h of milling. Additionally, for some quaternary alloys, a shoulder is clearly discernible at ~44.5° attributed to Fe(Ni) phase [4], suggesting that the mechanical alloying process between Cu, Ni and Fe is not fully completed.

After the consolidation procedure (Figure 1B), only one series of peaks attributed to the Cu(Ni,Fe,M) γ-phase is observed for M= Sn, V, Ir, and Ru, which tends to indicate that the alloying process has been completed during the consolidation procedure for these quaternary alloys. On the other hand, for M = Ag, Nb and Ta, small peaks of unalloyed M are discernible, suggesting that these elements are not fully dissolved in the γ phase. It can be explained by their larger atomic radius (1.43-1.44 Å) compared to that of Sn, V, Ir and Ru (1.40, 1.31, 1.36 and 1.33 Å, respectively). Note that unalloyed Nb and Ta are in oxide state, probably due to their reaction with residual O_2 during the consolidation step. Based on the position of the (111) peak of the γ-phase, an increase of the lattice parameter is observed for all quaternary alloys (3.607-3.625 Å compared to 3.599 Å for the Cu-Ni-Fe alloy, see Table 1), confirming the incorporation (complete or partial) of the M elements in the γ-phase. In addition, as expected, a decrease of the full width at half maximum (FWHM) of the diffraction peaks of the γ phase is observed due to grain growth and strain release. On the basis of Williamson-Hall plots (not shown), the crystallite size is ~60 nm and the lattice strain is ~0.3 % for the consolidated samples compared to ~20 nm and ~0.5% in the as-milled state.

Table 1. Lattice parameter of the γ-phase in the consolidated $Cu_{60}M_5Ni_{20}Fe_{15}$ samples.

M	Cu	Sn	Ag	V	Nb	Ir	Ru	Ta
a (Å)	3.599	3.625	3.613	3.606	3.607	3.607	3.608	3.607

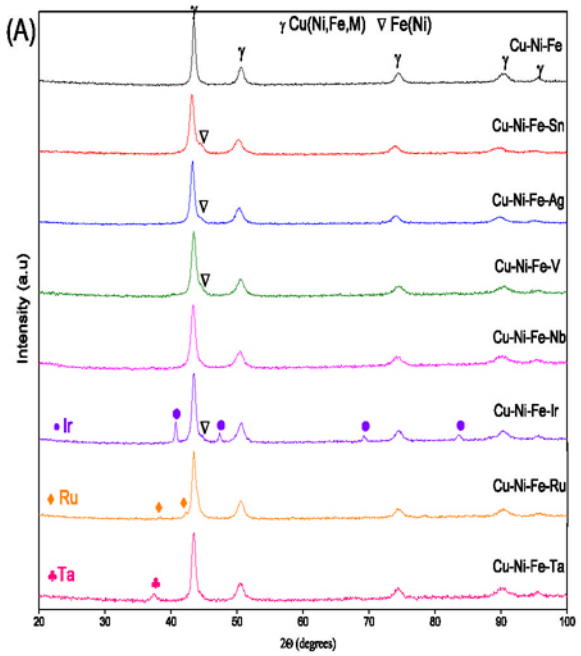

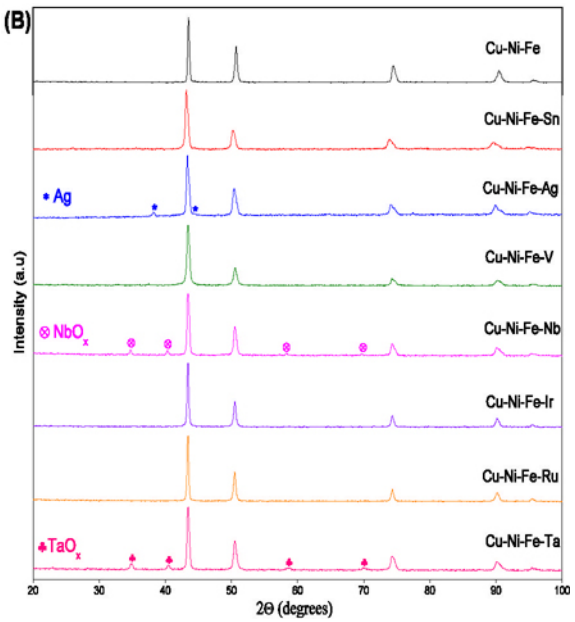

Figure 1. XRD patterns of the $Cu_{65}Ni_{20}Fe_{15}$ and $Cu_{60}M_5Ni_{20}Fe_{15}$ (M = Sn, Ag, V, Nb, Ir, Ru, Ta) materials in as-milled state (A) and after consolidation (B).

Figure 2 shows cross-section BSE micrographs and corresponding EDX mapping of the constitutive elements for the different consolidated $Cu_{60}M_5Ni_{20}Fe_{15}$ samples.

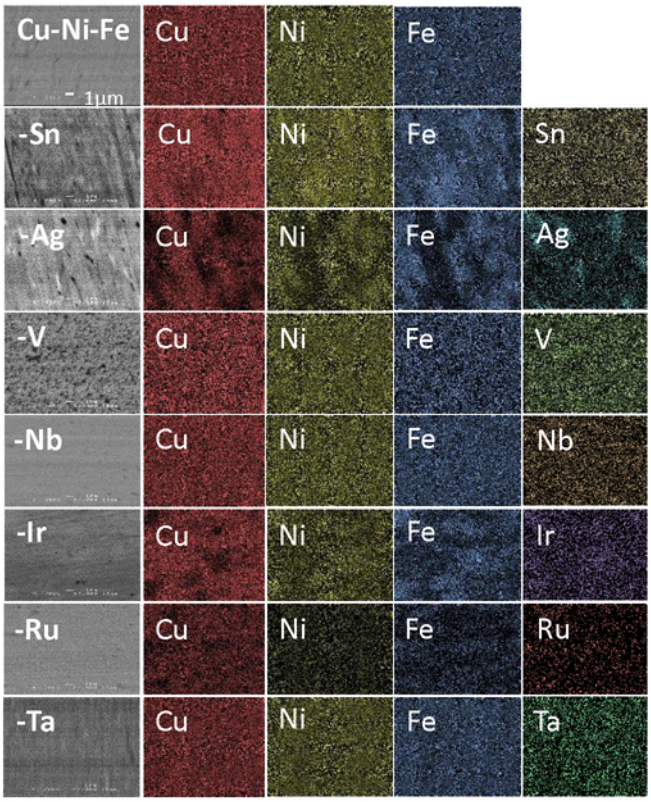

Figure 2. Cross-section BSE micrographs (x7000) and corresponding EDX mapping of the constitutive elements for the consolidated $Cu_{65}Ni_{20}Fe_{15}$ and $Cu_{60}M_5Ni_{20}Fe_{15}$ samples.

For the ternary Cu-Ni-Fe and quaternary Cu-Ni-Fe-M compounds with M = Nb and Ta, no apparent chemical segregation is observed. In contrast, with M = Sn, Ir, Ru and more especially with Ag, Cu-rich and Ni-Fe rich zones are discernible. This is usually observed on as-cast Cu-Ni-Fe alloys characterized by a dentritic microstructure made of Fe-Ni rich dendrites in a Cu-rich matrix, resulting from the alloy spinodal decomposition [9]. However, in this latter case, this dentritic microstructure is much more apparent on BSE micrographs, suggesting that the spinodal decomposition occurred on smaller scale for the present mechanically alloyed materials – this is expected due to the fact that the alloy was not heated during milling and the kinetics for spinodal decomposition are poor at low temperatures. Note that this phase decomposition is hardly detectable from XRD analyses due to the very close lattice constants of the Cu-rich and Fe-Ni-rich phases [10,11]. However, it may explain the small shoulder observed on the right of the peak at high diffraction angles in Figure 1B for some Cu-Ni-Fe-M compounds (more apparent for M = Ag). Regarding the dispersion of the M elements, discernible micrometric M-rich zones are only detected for M = Ag and V in Figure 2.

Figure 3 shows the TGA curves performed at 700°C under 1 atm Ar:O_2 (80:20) for 20 h on the $Cu_{65}Ni_{20}Fe_{15}$ and $Cu_{60}M_5Ni_{20}Fe_{15}$ pellets. The V-containing alloy displays the highest oxidation rate with a mass gain of 3% compared to ≤1.5% for the other alloys. The lowest oxidation rate is observed for M = Ir and Ag with a mass gain of ~0.65% versus 1.15% for the ternary Cu-Ni-Fe alloy. In most cases, a very rapid increase of the mass is observed during the first hour of oxidation, assumed to be mainly related to Cu oxidation. However, for M = Ru, Ir and Ag, this initial mass increase is much lower, suggesting that the formation of CuO_x is significantly slowed down in presence of these additional elements. Except for M = V, the oxidation rate drastically slows down for t > 1 h, which can be explained by the formation of $NiFe_2O_4$ acting as a barrier to the Cu flux at the oxide-alloy interface [12].

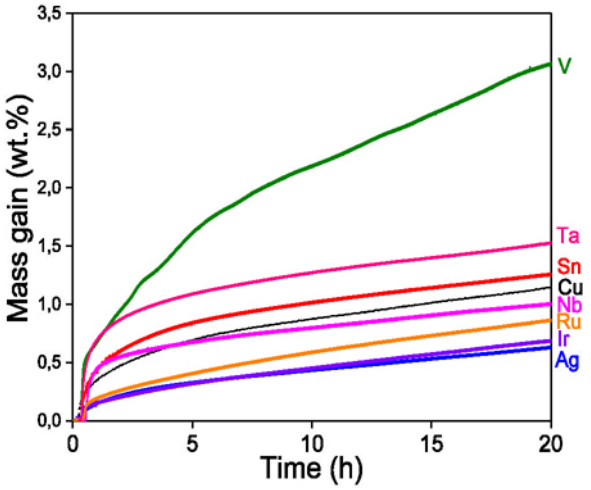

Figure 3. TGA curves of $Cu_{65}Ni_{20}Fe_{15}$ and $Cu_{60}M_5Ni_{20}Fe_{15}$ performed at 700°C under 1 atm Ar-20%O_2.

The XRD patterns of the samples after TGA are shown in Figure 4. In all cases, the formed oxides are mainly CuO and $NiFe_2O_4$. There is also Cu_2O for some samples (peaks at ~36 and ~42°for M= Cu, Sn, Ag and Ru). Note that the presence of NiO and Fe_3O_4 cannot be totally excluded on the basis of the present XRD analyses because their characteristic peaks closely overlap those of the $NiFe_2O_4$ phase. Except for M = V, peaks of the γ phase are also visible at 43.5 and 50.7°, which are more intense for M = Nb and Sn, suggesting the formation of a thinner oxide surface scale for these two alloys. Peaks related to MO_x phases are not discernable except for M= Sn in which SnO_2 phase is detected. This alloy also shows the presence of Fe_2O_3 phase. For M = Ag, peaks of Ag phase are observed.

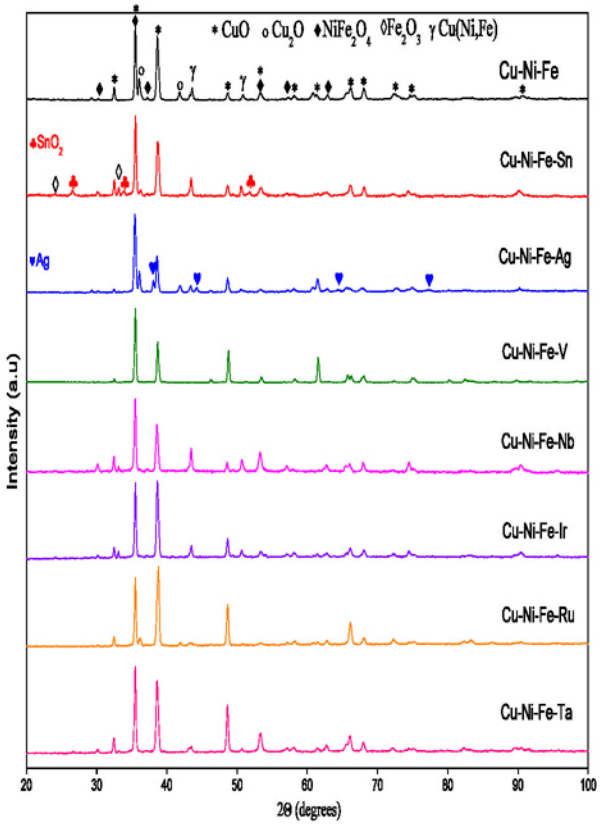

Figure 4. XRD patterns of the $Cu_{65}Ni_{20}Fe_{15}$ and $Cu_{60}M_5Ni_{20}Fe_{15}$ samples after TGA measurements.

The oxide scales formed of the $Cu_{65}Ni_{20}Fe_{15}$ and $Cu_{60}M_5Ni_{20}Fe_{15}$ samples were also characterized by cross-section BSE analyses and EDX mapping, as shown in Figure 5. Typically, the oxide scale formed on the different samples has a bilayer structure constituted of a CuO-rich outer layer and a $NiFe_2O_4$-rich inner layer. However, a major difference in their thicknesses is observed depending on the alloy composition. In accordance with TGA and XRD results, the thicker oxide layer is observed for M = V, with a total thickness of ~80 µm and the presence of porous and delaminated zones. For the ternary Cu-Ni-Fe alloy, the thicknesses of the outer CuO-rich layer and inner $NiFe_2O_4$-rich layer are both ~15µm, which are in the same order as observed for M = Ta and Ru. The thinnest oxide layer is observed for M = Nb, Ir, Ag and Sn with a total thickness ≤ 5-10µm. For M = Sn, a surface SnO_2-rich layer is also observed in contrast to the other quaternary Cu-Ni-Fe-M alloys where a MO_x layer is not clearly discernable. Ag inclusions dispersed in the bulk Cu-Ni-Fe-Ag alloy are also observed. Regarding the chemical homogeneity in the bulk alloy, the presence of Cu rich and Ni-Fe rich zones are clearly discernable for M= Ag. The presence of FeO_x which tends to segregate in inter-particle zones is observed for M = Ta, Ir and in a lesser extend for M = Cu and Sn. Actually, only the alloy with M = Nb seem to maintain a good chemical homogeneity in the bulk alloy zone.

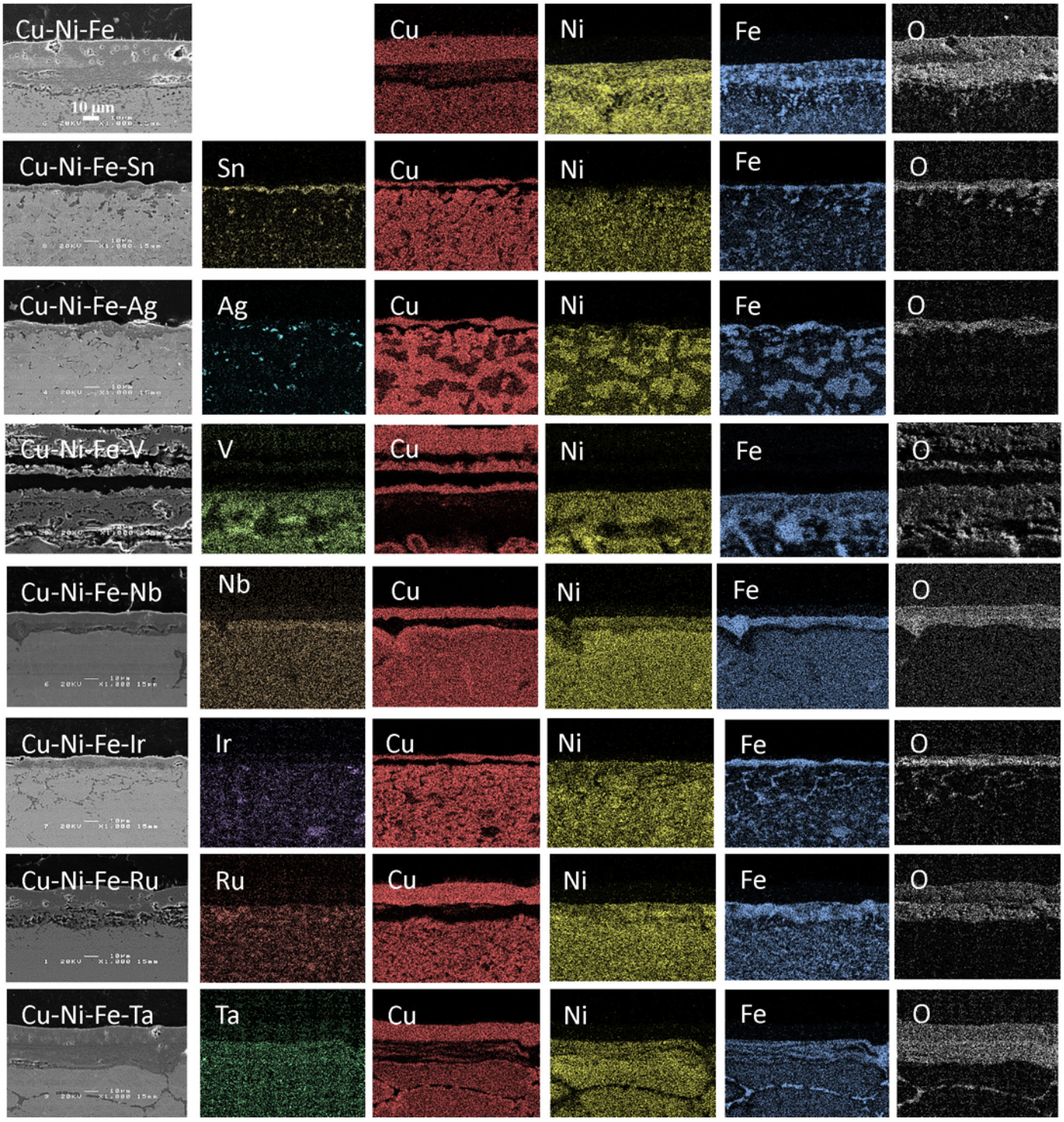

Figure 5. Cross-section BSE micrographs (x1000) and corresponding EDX mapping of the constitutive elements for the post-TGA $Cu_{65}Ni_{20}Fe_{15}$ and $Cu_{60}M_5Ni_{20}Fe_{15}$ samples.

Conclusion

This study showed that the substitution of 5 wt% of Cu by Sn, Ag, V, Nb, Ir, Ru or Ta in ball-milled $Cu_{65}Ni_{20}Fe_{15}$ alloy has a major effect on its high-temperature oxidation behavior by affecting the outward diffusion of Cu and the formation of Cu oxides. The best compromise in terms of oxide scale thinness and chemical homogeneity in the bulk alloy is observed for M = Nb. Further work is required to explain its distinctive behavior. Their evaluation under Al electrolysis conditions is also in progress to determine their resistance to fluorination, dissolution and electrolyte penetration.

References

1. T.R. Beck. A non-consumable metal anode for production of aluminum with low-temperature fluoride melts. Light Metals (1995) 355.
2. T. Nguyen et al. De Nora oxygen evolving inert metallic anode. Light Metals (2006) 385.
3. D.A. Simakov et al. Progress in the development of reduction technology with inert anodes. Proc. Non-Ferrous Metals (2012) 363.
4. S. Helle, M. Pedron, B. Assouli, B. Davis, D. Guay, L. Roué, Structure and high-temperature oxidation behavior of Cu-Ni-Fe based alloys prepared by high-energy ball milling for application as inert anodes for aluminum electrolysis. Corros. Sci. 52 (2010) 3348.
5. S. Helle, M. Tresse, D. Guay, L. Roué, Mechanically alloyed Cu-Ni-Fe-O based materials as oxygen-evolving anodes for aluminum electrolysis. J. Electrochem. Soc. 159 (2012) E62.
6. D.H. DeYoung. Solubilities of oxides for inert anodes in cryolite-based melts. Light Metals (1986) 299.
7. S.V. Divinski, C. Herzig, F. Hisker, R. Filipek, M. Danielewski, Self-and Interdiffusion in Ternary Cu-Fe-Ni Alloys. Defect and Diffusion Forum, 237-240 (2005) 50.
8. G. Goupil, S. Helle, B. Davis, D. Guay, L. Roué. Anodic behavior of mechanically alloyed Cu-Ni-Fe and Cu-Ni-Fe-O electrodes for aluminum electrolysis in low-temperature KF-AlF_3 electrolyte. Electrochim. Acta 112 (2013) 176.
9. I. Gallino, M.E. Kassner, and R. Bush. Oxidation and corrosion of highly alloyed Cu–Fe–Ni as inert anode material for aluminum electrowinning in as-cast and homogenized conditions. Corros. Sci. 63 (2012) 293.
10. M. Baricco, E. Bosco, G. Acconciaioco, P. Rizzi, M. Coisson. Rapid solidification of Cu-Ni-Fe alloys. Mater. Sci. Eng. A 375-377 (2004) 1019.
11. K.P. Gupta, S.B. Rajendraprasad, A.K. Jena. The copper-iron-nickel system. J. Alloys Phase Diagrams 3 (1987) 116.
12. R. Haugsrud, T. Norby, P. Kofstad. High-Temperature Oxidation of Cu-30Ni-15Fe. Corros. Sci. 43 (2001) 283.